Atmos. Chem. Phys. Discuss., 13, 26305–26325, 2013
www.atmos-chem-phys-discuss.net/13/26305/2013/
doi:10.5194/acpd-13-26305-2013

Atmospheric Chemistry and Physics Discussions

Measuring the Antarctic ozone hole with the new Ozone Mapping and Profiler Suite (OMPS)

N. A. Kramarova[1], E. R. Nash[1], P. A. Newman[2], P. K. Bhartia[2], R. D. McPeters[2], D. F. Rault[3], C. J. Seftor[1], and P. Q. Xu[4]

[1]Science Systems and Applications, Inc., Lanham, Maryland, USA
[2]NASA Goddard Space Flight Center, Greenbelt, Maryland, USA
[3]Morgan State University, Baltimore, Maryland, USA
[4]Science Applications International Corp., Beltsville, Maryland, USA

Received: 7 August 2013 – Accepted: 14 September 2013 – Published: 10 October 2013

Correspondence to: N. A. Kramarova (natalya.a.kramarova@nasa.gov)

Published by Copernicus Publications on behalf of the European Geosciences Union.

Abstract

The new Ozone Mapping and Profiler Suite (OMPS) launched on the Suomi National Polar-orbiting Partnership satellite in October 2011 gives a more detailed view of the development of the Antarctic ozone hole than ever before. This instrumental suite extends the long series of satellite ozone measurements that go back to the early 1970s. The OMPS includes two modules – nadir and limb – to measure profile and total ozone concentrations. The new limb module is designed to measure the vertical profile of ozone between the lowermost stratosphere and the mesosphere. The OMPS observations over Antarctica show excellent agreement with the measurements obtained from independent satellite and ground-based instruments. This validation demonstrates that OMPS data can ably extend the ozone time series over Antarctica in the future. The OMPS observations are used to monitor and characterize the evolution of the 2012 Antarctic ozone hole. While large ozone losses were observed in September 2012, a strong ozone rebound occurred in October and November 2012. This ozone rebound is characterized by rapid increases of ozone at mid-stratospheric levels and a splitting of the ozone hole in early November. The 2012 Antarctic ozone hole was the second smallest on record since 1988.

1 Introduction

Since the middle of the 1980s, when the Antarctic ozone hole was first discovered (Farman et al., 1985; Stolarski et al., 1986), severe ozone depletion has been observed every austral spring over the Antarctic region. The levels of ozone depleting substances (ODS) and the specific meteorological conditions control the development of the seasonal Antarctic ozone hole (WMO, 2007). The rapid ozone depletion in the spring, caused by heterogenous chemical reactions, results in significant ozone loss at around 70 hPa in October, with the depletion up to 98 % compared to the early 1970s period as observed over South Pole and Syowa stations (Solomon et al., 2005). The

ACPD
13, 26305–26325, 2013

lowest total ozone concentration and the area of the Antarctic ozone hole, however, vary from year to year (WMO, 2011). In 2002 the unique dynamical situation resulted in the first sudden stratospheric warming ever observed in the Southern Hemisphere (Newman and Nash, 2005). This situation led to the unusually high ozone concentration over Antarctica in 2002, despite high levels of ODSs.

Recently the levels of ODSs, primarily comprised of chlorine- and bromine-containing chemicals (Newman et al., 2007), have started to decline (Solomon et al., 2006; Jones et al., 2011; WMO, 2011) as a result of the Montreal Protocol regulations. Some studies (e.g., Salby et al., 2011, 2012) have claimed that there is an upward ozone trend over the last decade in Antarctica. However, Hassler et al. (2011) showed that the first signs of ozone recovery will not be detectable earlier than 2017–2021, based on the analysis of ozonesonde measurements at South Pole station. Hence, the continuation of satellite observations over Antarctica are critical in the next decades as the ozone hole is expected to show signs of recovery due to declining concentrations of ODSs.

Prior satellite instruments to measure profile and total column ozone have included the Total Ozone Mapping Spectrometer (TOMS), the Solar Backscatterd Ultraviolet instrument (SBUV/2), and the Ozone Monitoring Instrument (OMI). The Ozone Mapping and Profiler Suite (OMPS) represents the next generation of the US ozone monitoring system (Flynn et al., 2006). OMPS was designed to provide profile and total ozone products that meet the stringent requirements needed both for operational uses and to continue the long-term historical records. The OMPS instrumental suite began routine operations in 2012.

This study uses OMPS profile and total ozone observations to determine the temporal and spatial evolution of the 2012 Antarctic ozone hole. The main focus is to validate OMPS ozone observations and to demonstrate the benefits of the synthesis of the three-instrument suite for more detailed monitoring of the Antarctic ozone hole.

The rest of this study is organized into four additional sections. A brief description of OMPS instruments is presented in Sect. 2. Section 3 shows results of the compar-

ACPD
13, 26305–26325, 2013

ison of the OMPS observations over Antarctica against independent measurements. Section 4 investigates results of monitoring the 2012 ozone hole using OMPS measurements, including estimates of the lowest ozone concentration and the hole area. Conclusions are presented in Sect. 5.

2 The Ozone Mapping and Profiler Suite

OMPS was launched on 28 October 2011 on the Suomi National Polar-orbiting Partnership satellite. The OMPS sensor suite has both nadir and limb modules. The nadir module combines two sensors: Total Column Nadir Mapper (TC-NM) for measuring total column ozone, and the Nadir Profiler (NP) for ozone vertical profiles. The Limb Profiler (LP) module is designed to measure vertical ozone profiles with good vertical resolution (1–3 km) from the upper troposphere/lower stratosphere to the mesosphere. These modules are based on heritage designs: the OMPS TC-NM is similar to TOMS and OMI, the OMPS NP is similar to SBUV/2, and the OMPS LP is similar to the Shuttle Ozone Limb Sounding Experiment flown on STS-87 and STS-107.

Both nadir sensors (TC-NM and NP) measure the ultraviolet radiance backscattered by the Earth's atmosphere and surface, and they share some optical elements. The primary change in the OMPS nadir sensors is a switch from the traditional photomultiplier used previously in TOMS and SBUV/2 to a charge-coupled device (CCD) (Flynn et al., 2006).

The OMPS TC-NM sensor has a 110° cross-track field-of-view (FOV), with 35 cross-track bins, and a 0.27° along-track slit width corresponding to a 50 km resolution. The TC-NM has 300–400 nm spectral coverage. The OMPS TC-NM algorithm is very similar to the NASA Version 8 TOMS algorithm used for OMI (Bhartia and Wellemeyer, 2002). The basic algorithm uses two wavelengths to derive total ozone: one wavelength with weak ozone absorption to characterize the underlying surface and clouds, and the other with stronger ozone absorption and sensitivity to the total column. The

ACPD
13, 26305–26325, 2013

OMPS TC-NM algorithm uses ozone absorption cross sections based on Brion et al. (1993), whereas OMI and TOMS use older cross sections from Bass and Paur (1985).

The OMPS NP sensor has a 16.6° cross-track FOV and a 0.26° along-track slit width, giving cells of size 250 km by 250 km collocated with five central cells of the OMPS TC-NM sensor. The OMPS NP has spectral coverage of 250–310 nm. The OMPS NP retrieval algorithm (by analogy with SBUV/2) uses 12 discrete wavelengths to retrieve ozone profiles employing the maximum likelihood (or optimal estimation) technique (Bhartia et al., 2013). Though the vertical resolution of the OMPS NP ozone retrievals is coarse, this sensor provides valuable middle stratosphere to mesosphere profiles, data for the continuation of the SBUV/2 data record, and validation of the OMPS LP retrievals.

The OMPS LP measures solar radiances scattered from the atmosphere limb in the ultraviolet (UV) and visible spectral ranges. The UV wavelength measurements provide information about ozone concentration in the upper and middle stratosphere whereas visible wavelength measurements provide information on the lower stratosphere (McPeters et al., 2000). The OMPS LP has three slits separated horizontally by 4.25° (about 250 km) to expand the sensor cross-track coverage. Each slit provides a 1.85° vertical FOV (corresponding to 112 km vertical extent at the tangent point), allowing for atmospheric coverage of 0–60 km plus an offset allowance. The OMPS LP splits each vertical profile into two images: low altitude (bright) signals are measured with the small aperture, whereas the high altitude (low intensity) signals are measured with the large aperture. Measurements at short and long integration times are interleaved over the nominal 19 s measurement duration (Jaross et al., 2012). All six spectra (three slits and two apertures) are captured onto a single focal plane. Three ozone profiles (one for each slit) are produced every 19 s, which corresponds to a 1° latitude sampling. To minimize the sensitivity to the underlying scene reflectance, measured radiances are first normalized with radiances measured at high altitudes (at 65 km in the UV and at 45 km in the visible). The LP ozone retrieval algorithm uses the pair/triplet method (Flittner et al., 2000; Rault, 2005).

ACPD
13, 26305–26325, 2013

3 Validation of OMPS measurements

OMPS measurements show excellent consistency both internally between modules and with other satellites. Figure 1 shows the validation of the measurements from the OMPS sensors over a 3 month time period in September–November 2012 in the 55° S–82° S latitude band. OMPS LP data (version 1) are reported as number densities (molecules cm^{-3}) at 81 altitude levels with a step of 1 km. Only profiles obtained from the central slit are considered in this study, and altitude range is limited from 14 km to about 50 km. OMPS NP data (version 1, NASA research processing) are reported as partial ozone columns (DU $layer^{-1}$) in 21 SBUV/2 pressure layers. To compare OMPS LP and OMPS NP profiles the OMPS LP number densities are converted into partial ozone columns on the SBUV/2 grids. There is a good agreement between OMPS LP and OMPS NP measurements with the mean biases within ±6 % (Fig. 1a, blue). The standard deviation of the differences (Fig. 1b, blue) is less than 5 % between 1 hPa and 10 hPa and increases below this pressure range due to coarser OMPS NP vertical resolution in the lower stratosphere and troposphere. These results demonstrate a high consistency among the measurements obtained from OMPS LP and OMPS NP.

In addition, OMPS LP and OMPS NP measurements are compared against independent satellite observations: the Aura Microwave Limb Sounder (MLS), and the SBUV/2 instrument on board the NOAA-18 and NOAA-19 satellites. SBUV/2 has the same vertical resolution as OMPS NP and measurements can be compared directly. Comparisons of SBUV/2 (version 8.6) against OMPS NP demonstrate a good agreement with the biases of 2–4 % between 25 hPa and 1 hPa and standard deviations of 5–10 % (Fig. 1a and Fig. 1b, red and green). Figure 1c shows results of the comparison between OMPS LP and Aura MLS (version 3.3). The OMPS LP number densities are converted into mixing ratios using National Centers for Environmental Prediction – Department of Energy AMIP-II Reanalysis temperature profiles and MLS mixing ratio profiles are interpolated onto the OMPS LP vertical grids. The mean differences are within ±5 % between 16 km and 48 km. The standard deviations are about 10 % be-

ACPD
13, 26305–26325, 2013

tween 24 km and 48 km and increase below and above these levels (up to 50 % in the lower stratosphere).

Figure 2 shows validations of OMPS LP ozone profiles in the lower stratosphere against Neumayer Station (70° S, 8° W) ozonesonde measurements. There are 36 balloon observations at Neumayer in the considered 3 month time period. Both OMPS LP and Aura MLS overestimate ozone concentration compared to sondes throughout the entire altitude range from 14 km to 30 km. Biases are 5 % or less above 21 km, but are significantly larger (up to 10–20 %) in the lower stratosphere between 14 km and 21 km. The standard deviations of the differences also increase in this layer (Fig. 2b). The black line in Fig. 2b shows the standard deviations of sonde measurements around the time mean and indicates greater ozone variability in the altitude range between 14 km and 21 km. Between 16 km and 22 km OMPS LP agrees better with sondes than Aura MLS, but between 14 km and 16 km OMPS LP overestimates ozone concentration relative to both. Both satellite instruments, OMPS LP and Aura MLS, demonstrate a similar behavior in the lower stratosphere as compared with balloon measurements (Fig. 2c and Fig. 2d).

Total ozone columns measured by OMPS TC-NM and OMPS NP are validated against the corresponding independent observations obtained from SBUV/2. Mean biases are less than 1 % with standard deviations of 3–4 %. The validation of OMPS total ozone and profile measurements against measurements from these other satellites demonstrate good agreement and indicate that the OMPS instruments provide very reasonable estimates of Antarctic ozone concentrations.

4 OMPS ozone hole first results

Large depletions of total ozone over Antarctica have been routinely observed by satellites since the discovery of the ozone hole in 1985 (Farman et al., 1985; Stolarski et al., 1986). The OMPS TC-NM observations from 2012 continue that time series. Figure 3 shows that the differences in the monthly mean October 2012 ozone amounts between

ACPD
13, 26305–26325, 2013

OMI and OMPS TC-NM are relatively small, ranging from −2.4 % to 4.3 %. OMPS is generally higher everywhere, but lower near and within the ozone hole region. These differences are quite small in comparison to the levels of column ozone loss that have been observed over Antarctica (> 50 %).

One of the primary metrics for assessing ozone depletion is the area contained within the 220 DU contour during the period from 7 September to 13 October. Figure 4 shows the area over this period for the years from 1979 through 2012. Two 2012 values are plotted: the OMI estimate of 17.8 million km^2 (black) and the OMPS TC-NM estimate of 17.6 million km^2 (red). The 2012 range of daily values for OMPS (red) is 10.8–20.9 million km^2, while the range for OMI (black) is 11.2–21.1 million km^2. The plot reveals two interesting aspects. First, the 2012 area was one of the smallest on record since the early 1990s. Only the 2002 area was smaller – a year with the first observed major sudden stratospheric warming in the Southern Hemisphere (Newman and Nash, 2005). Second, the area shows a slight downward trend over the 1995–2012 period, visually suggesting that the Antarctic ozone hole may be recovering.

During 2012, the ozone hole area increased normally during the August to early-September period, but diminished quite rapidly during the late-September to October period (compared to the last 20 yr period). Figure 5a shows the daily estimates of the ozone hole area from the OMPS TC-NM (red) and OMI (blue). After removing the seasonal cycle, the standard deviation of the area is 2.90×10^6 km^2 and the standard error between OMPS TC-NM and OMI is 0.68×10^6 km^2. The OMPS TC-NM is correlated at the 0.97 level with OMI.

As with the area, the minimum value of ozone fell at a somewhat slower rate in 2012, but stopped decreasing in about mid-September. Minimum values recovered more quickly than normal in October and were above normal levels by early December. Again, the OMPS TC-NM and OMI minimum values were in close agreement. After removing the annual cycle from the data in Fig. 5b, the standard deviation of the minimums is 19.9 DU and the standard error between OMI and OMPS is 4.8 DU.

ACPD
13, 26305–26325, 2013

Figure 6 shows the evolution of the 2012 Antarctic ozone hole. Total column ozone and ozone mixing ratios are chosen near the center of the polar vortex (Fig. 6a and Fig. 6b). The polar vortex is defined by NASA Global Modeling and Assimilation Office Modern Era Retrospective-Analysis for Research and Applications (GMAO MERRA) potential vorticity on the 460 K potential temperature surface. The location of the lowest total ozone near the center of the vortex, consistent with a smooth transition from day to day, is chosen for each day (see locations in Fig. 6c). During the vortex split in early November, the "blob" of vortex air that maintains itself the longest is followed. The vortex center remains in the range of −120° E to −30° E until the middle of October, then moves eastward through the vortex splitting, and ends up back in the same range in November as where it started in September.

Figure 6a (also Fig. 5b) shows that minimum total ozone occurs on 1 October and then increases through the October–November period. As has been shown by Hassler et al. (2011), there is a strong vertical gradient of ozone near 20 km (Fig. 6b). This gradient results from the very strong ozone depletion that occurs at altitudes below 22 km. The minimum value in the profile occurs around 15 km – about 10 days after the total column minimum. There is a general steady increase in ozone at all levels starting from early October and proceeding through the end of November. The most dramatic increase occurs in the 25–30 km range, where mixing ratios almost double over this time period. Increases are much more modest in the lower stratosphere and level off by the middle of November.

The progression of ozone values during the austral spring is shown in Fig. 7 for both total column ozone (bottom row) and for three layers of the lower stratosphere. The gray vertical lines in Fig. 6 indicate days that are shown in Fig. 7. The white circles in Fig. 7 surround the point of the vortex used in the bottom panel of Fig. 6. On 2 September the ozone partial column values in the two upper levels correspond well to the total column ozone, while the lower-level ozone amounts are relatively high. By 19 September the partial column values are being depleted at all levels, and the ozone hole indicated by the total column shows deepening (bottom). By 4 October, near the

ACPD
13, 26305–26325, 2013

minimum in total column ozone, all levels have had significant partial column value decreases, especially in the lowest layer.

The ozone hole area rapidly decreases in October and then splits into two parts. Note that the size of the low ozone area in the 26.5–29.5 km panels of Fig. 7 show a steady decline through the 2 September to 21 November period. There is also a strong wave-1 warming event in October that displaces the vortex and the ozone hole off of the pole. By 19 October the partial column values at the upper levels are starting to increase, while the lowest level retains low values. In early November a strong wave-2 warming event splits the vortex and the ozone hole into two parts. The partial column values continue to increase at the upper levels through the end of November, while the partial column values at lower levels remain about the same.

Some have implied that the smaller ozone hole area results from a decrease in chlorine in the stratosphere (Salby et al., 2012). However, to first order, the smaller size appears to result from dynamical effects and not chlorine decreases. Inspection of Fig. 5 shows that the ozone hole develops at the same rate as in previous years during the August and early-September period. This is the period when chlorine chemical effects are most prominent (Kawa et al., 2009). Both the area and minimum values indicate a more rapid than normal ozone hole recovery in the late-September through November period. Strong wave events revealed in both the ozone distributions (wave-2 split in Fig. 7), and dynamical proxies such as the Eliassen–Palm flux (not shown) indicate that this more rapid recovery is dynamically driven.

5 Summary and conclusions

The OMPS suite began routine operations in 2012. OMPS follows from the strong heritage of UV-visible satellite instruments that extend from the 1970s. OMPS is now the standard ozone-monitoring instrument aboard the US polar orbiting satellites.

Comparisons of OMPS observations in the Antarctic region to standard measurements show that OMPS performs quite reasonably. First, direct comparisons of OMPS

ACPD
13, 26305–26325, 2013

TC-NM and OMPS NP to the SBUV/2 column observations show differences of < 1 %. Second, the comparison of the OMPS profilers to the Aura MLS, SBUV/2, and ozonesondes shows good agreement between profiles from the upper stratosphere to the lowermost stratosphere (13–45 km). These comparisons give us good confidence in the ability of OMPS instruments to monitor the characteristics of the Antarctic ozone hole.

Estimates of ozone hole diagnostics from OMPS TC-NM are in excellent agreement with OMI observations. The estimates of the ozone hole's average size is within 0.2 million km^2, while the value of the average minimum is within 1.2 DU. These excellent comparisons show that OMPS can continue the long-term Antarctic ozone hole time series. This continuation is critical for the next decade as the ozone hole begins to show signs of recovery.

The ozone hole developed quite normally in 2012, but because of the strong wave dynamics, faster warming during austral spring, and stronger advection, the 2012 ozone hole disappeared quite rapidly during the late-September to November period as compared to the ozone holes of the last 20 yr. This resulted in the second weakest ozone hole observed since 1988. The weakest ozone hole observed in this period was 2002 – driven by the first observed major stratospheric sudden warming in the Southern Hemisphere. The date of the ozone hole disappearance was also one of the earliest on record. The wave dynamics resulted in a splitting of the ozone hole during the early-November period (similar to the situation observed in late-September 2002). Because the development of the ozone hole in August and September is largely driven by the amounts of chlorine and bromine, the normal development of the ozone hole in August–September 2012 suggests that the ozone hole is not currently demonstrating a response to ODS declines, but is rather driven by the strong wave dynamics.

Acknowledgements. This work was supported under the NASA Atmospheric Chemistry Modeling and Analysis Program and the Modeling, Analysis, and Prediction Program. The Aura MLS science teams provided the high quality satellite ozone data set. The World Ozone and Ultraviolet Radiation Data Center (WOUDC) provided ozonesonde data. OMPS data are available

ACPD
13, 26305–26325, 2013

at http://ozoneaq.gsfc.nasa.gov/omps. The MERRA data have been provided by the Global Modeling and Assimilation Office (GMAO) at NASA Goddard Space Flight Center through the NASA GES DISC online archive (http://disc.sci.gsfc.nasa.gov/daac-bin/DataHoldings.pl).

References

Bass, A. M. and Paur, R. J.: The ultraviolet cross-sections of ozone: I. the measurements, in: Atmospheric Ozone: Proceedings of the Quadrennial Ozone Symposium Halkidiki, Greece, 3–7 September 1984, edited by: Zerefos, C. S. and Ghazi, A., Reidel, Dordrecht, the Netherlands, 606–610, 1985. 26309

Bhartia, P. K. and Wellemeyer, C. W.: TOMS-V8 total O_3 algorithm, in: OMI Algorithm Theoretical Basis Document: OMI Ozone Products, edited by: Bhartia, P. K., ATBD-OMI-02, 15–32, available at: http://www.knmi.nl/omi/documents/data/OMI_ATBD_Volume_2_V2.pdf, 2002. 26308

Bhartia, P. K., McPeters, R. D., Flynn, L. E., Taylor, S., Kramarova, N. A., Frith, S., Fisher, B., and DeLand, M.: Solar Backscatter UV (SBUV) total ozone and profile algorithm, Atmos. Meas. Tech., 6, 2533–2548, doi:10.5194/amt-6-2533-2013, 2013. 26309

Brion, J., Chakir, A., Daumont, D., Malicet, J., and Parisse, C.: High-resolution laboratory absorption cross section of O_3: temperature effect, Chem. Phys. Lett., 213, 610–612, doi:10.1016/0009-2614(93)89169-I, 1993. 26309

Farman, J. C., Murgatroyd, R. J., Silnickas, A. M., and Thrush, B. A.: Ozone photochemistry in the Antarctic stratosphere in summer, Q. J. Roy. Meteor. Soc., 111, 1013–1028, doi:10.1002/qj.49711147006, 1985. 26306, 26311

Flittner, D. E., Herman, B. M., and Bhartia, P. K.: O_3 profiles retrieved from limb scatter measurements: theory, Geophys. Res. Lett., 27, 2601–2604, doi:10.1029/1999GL011343, 2000. 26309

Flynn, L. E., Seftor, C. J., Larsen, J. C., and Xu, P.: The Ozone Mapping and Profiler Suite, in: Earth Science Satellite Remote Sensing, edited by: Qu, J. J., Gao, W., Kafatos, M., Murphy, R. E., and Salomonson, V. V., Springer, Berlin, 279–296, doi:10.1007/978-3-540-37293-6, 2006. 26307, 26308

ACPD
13, 26305–26325, 2013

Hassler, B., Daniel, J. S., Johnson, B. J., Solomon, S., and Oltmans, S. J.: An assessment of changing ozone loss rates at South Pole: twenty-five years of ozonesonde measurements, J. Geophys. Res., 116, D22301, doi:10.1029/2011JD016353, 2011. 26307, 26313

Jaross, G., Chen, G., Kowitt, M., Warner, J., Xu, P., Kelly, T., Linda, M., and Flittner, D.: Suomi NPP OMPS Limb Profiler initial sensor performance assessment, in: Proc. SPIE 8528, Earth Observing Missions and Sensors: Development, Implementation, and Characterization II, 852805, 28 November 2012, doi:10.1117/12.979627, 2012. 26309

Jones, A., Urban, J., Murtagh, D. P., Sanchez, C., Walker, K. A., Livesey, N. J., Froidevaux, L., and Santee, M. L.: Analysis of HCl and ClO time series in the upper stratosphere using satellite data sets, Atmos. Chem. Phys., 11, 5321–5333, doi:10.5194/acp-11-5321-2011, 2011. 26307

Kawa, S. R., Stolarski, R. S., Newman, P. A., Douglass, A. R., Rex, M., Hofmann, D. J., Santee, M. L., and Frieler, K.: Sensitivity of polar stratospheric ozone loss to uncertainties in chemical reaction kinetics, Atmos. Chem. Phys., 9, 8651–8660, doi:10.5194/acp-9-8651-2009, 2009. 26314

McPeters, R. D., Janz, S. J., Hilsenrath, E., Brown, T. L., Flittner, D. E., and Heath, D. F.: The retrieval of O_3 profiles from limb scatter measurements: results from the Shuttle Ozone Limb Sounding Experiment, Geophys. Res. Lett., 27, 2597–2600, doi:10.1029/1999GL011342, 2000. 26309

Newman, P. A. and Nash, E. R.: The unusual Southern Hemisphere stratospheric winter of 2002, J. Atmos. Sci., 62, 614–628, doi:10.1175/JAS-3323.1, 2005. 26307, 26312

Newman, P. A., Daniel, J. S., Waugh, D. W., and Nash, E. R.: A new formulation of equivalent effective stratospheric chlorine (EESC), Atmos. Chem. Phys., 7, 4537–4552, doi:10.5194/acp-7-4537-2007, 2007. 26307

Newman, P. A., Kramarova, N., Nash, E. R., Long, C. S., Pitts, M. C. Johnson, B., Santee, M. L., Burrows, J., and Braathen, G. O.: Ozone depletion, in State of the climate in 2012, B. Am. Meteorol. Soc., 94, S142–S146, doi:10.1175/2013BAMSStateoftheClimate.1, 2013. 26324

Rault, D. F.: Ozone profile retrieval from Stratospheric Aerosol and Gas Experiment (SAGE III) limb scatter measurements, J. Geophys. Res., 110, D09309, doi:10.1029/2004JD004970, 2005. 26309

Salby, M., Titova, E., and Deschamps, L.: Rebound of Antarctic ozone, Geophys. Res. Lett., 38, L09702, doi:10.1029/2011GL047266, 2011. 26307

ACPD
13, 26305–26325, 2013

Salby, M. L., Titova, E. A., and Deschamps, L.: Changes of the Antarctic ozone hole: controlling mechanisms, seasonal predictability, and evolution, J. Geophys. Res., 117, D10111, doi:10.1029/2011JD016285, 2012. 26307, 26314

Solomon, P., Barrett, J., Mooney, T., Connor, B., Parrish, A., and Siskind, D. E.: Rise and decline of active chlorine in the stratosphere, Geophys. Res. Lett., 33, L18807, doi:10.1029/2006GL027029, 2006. 26307

Solomon, S., Portmann, R. W., Sasaki, T., Hofmann, D. J., and Thompson, D. W. J.: Four decades of ozonesonde measurements over Antarctica, J. Geophys. Res., 110, D21311, doi:10.1029/2005JD005917, 2005. 26306

Stolarski, R. S., Kreuger, A. J., Schoeberl, M. R., McPeters, R. D., Newman, P. A., and Alpert, J. C.: Nimbus-7 satellite measurements of the springtime Antarctic ozone decrease, Nature, 322, 808–811, doi:10.1038/322808a0, 1986. 26306, 26311

World Meteorological Organization (WMO): Scientific Assessment of Ozone Depletion: 2006, Global Ozone Res. Mon. Proj., Report No. 50, 572 pp., Geneva, Switzerland, 2007. 26306

World Meteorological Organization (WMO): Scientific Assessment of Ozone Depletion: 2010, Global Ozone Res. Mon. Proj., Report No. 52, 516 pp., Geneva, Switzerland, 2011. 26307

ACPD
13, 26305–26325, 2013

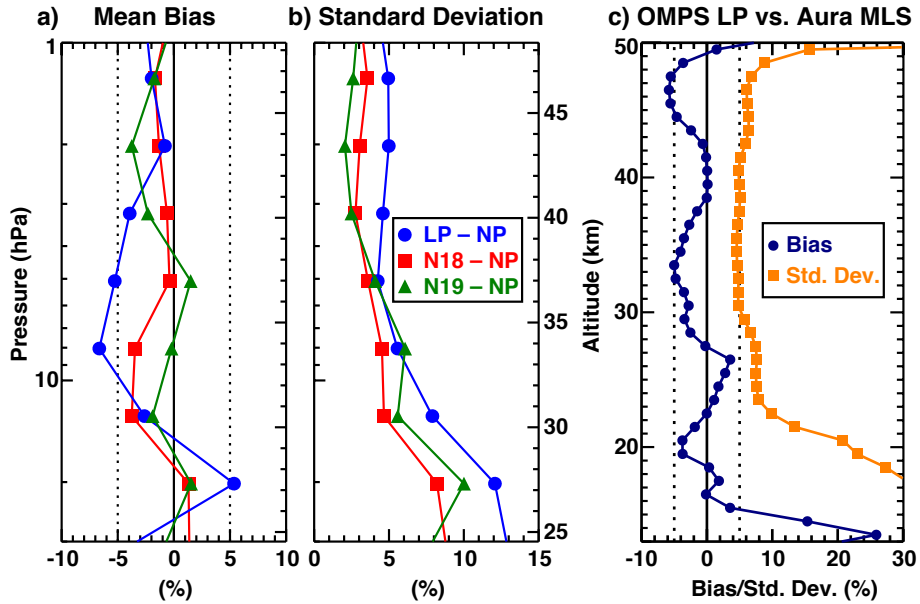

Fig. 1. Vertical profiles of the mean differences **(a)** and corresponding standard deviations of the differences **(b)** for OMPS LP (blue), SBUV/2 NOAA18 (red), and NOAA19 (green) against OMPS NP. Vertical profiles of mean differences (navy line) and standard deviations (orange line) for comparisons between OMPS LP and Aura MLS **(c)**. All data were compared over a 3 month period September–November 2012 in the latitude band 55° S–82° S. Spatial coincidence criteria are ±1° latitude and ±4° longitude. Temporal criteria are different for each pair of instruments: ±0.5 h for OMPS LP and OMPS NP, ±1 h for OMPS LP and Aura MLS, and ±4 h for SBUV/2 (NOAA 18 and NOAA 19) and OMPS NP comparisons.

ACPD
13, 26305–26325, 2013

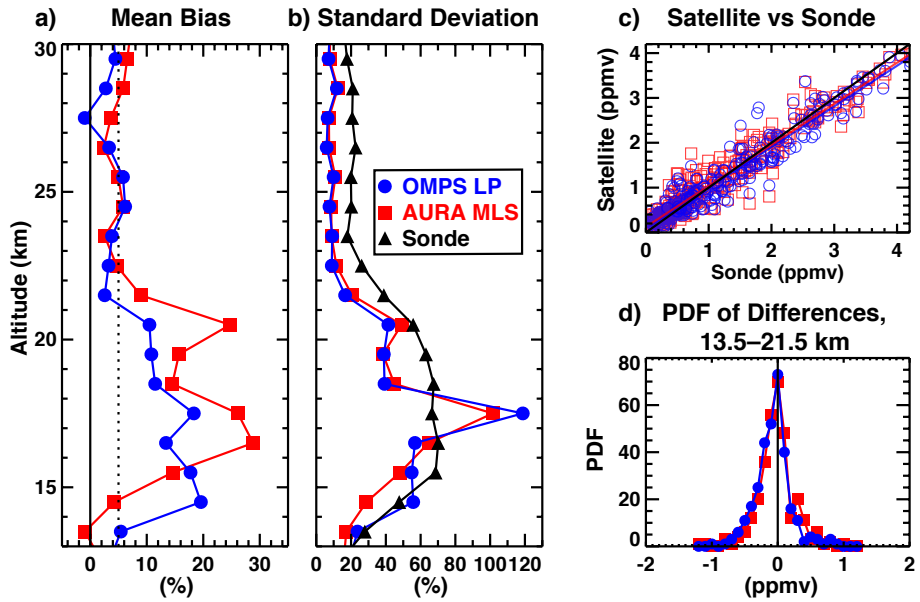

Fig. 2. Comparison of OMPS LP and Aura MLS against the ozonesonde balloon measurements from Neumayer (70° S, 8° W) for September–November 2012. Vertical profiles of mean differences **(a)** and standard deviations for OMPS LP (blue) and Aura MLS (red) relative to the sonde measurements **(b)**. Standard deviations of the sonde measurements relative to their time mean are also shown (black). OMPS LP and Aura MLS vs. the sonde measurements in layers between 13.5 km and 21.5 km **(c)**. Probability density functions of the differences for OMPS LP and Aura MLS relative to the sonde measurements in layers between 13.5 km and 21.5 km **(d)**.

ACPD
13, 26305–26325, 2013

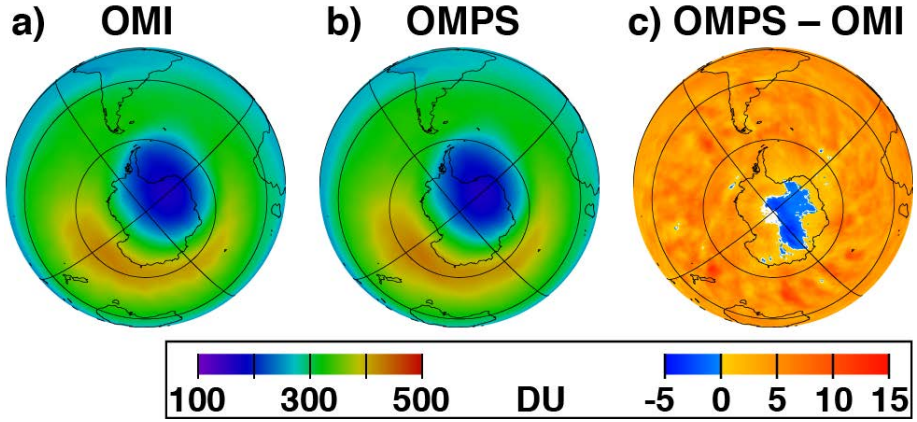

Fig. 3. Total column ozone from OMI **(a)**, OMPS TC-NM **(b)**, and their difference (OMPS−OMI) **(c)** for October 2012.

ACPD
13, 26305–26325, 2013

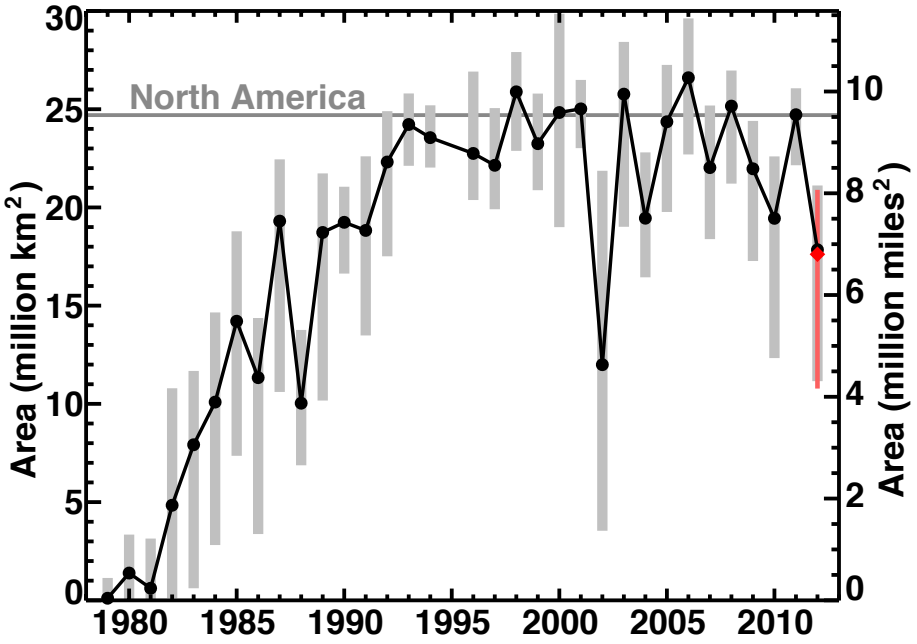

Fig. 4. Area of the Antarctic ozone hole from TOMS and OMI measurements (black circles), 1979–2012, and from OMPS (red circle) for 2012. These values are averaged from daily total ozone area values contained by the 220 DU contour for 7 September to 13 October. The range of these daily total ozone area values are indicated for TOMS and OMI (gray shading) and OMPS (red shading in 2012).

ACPD
13, 26305–26325, 2013

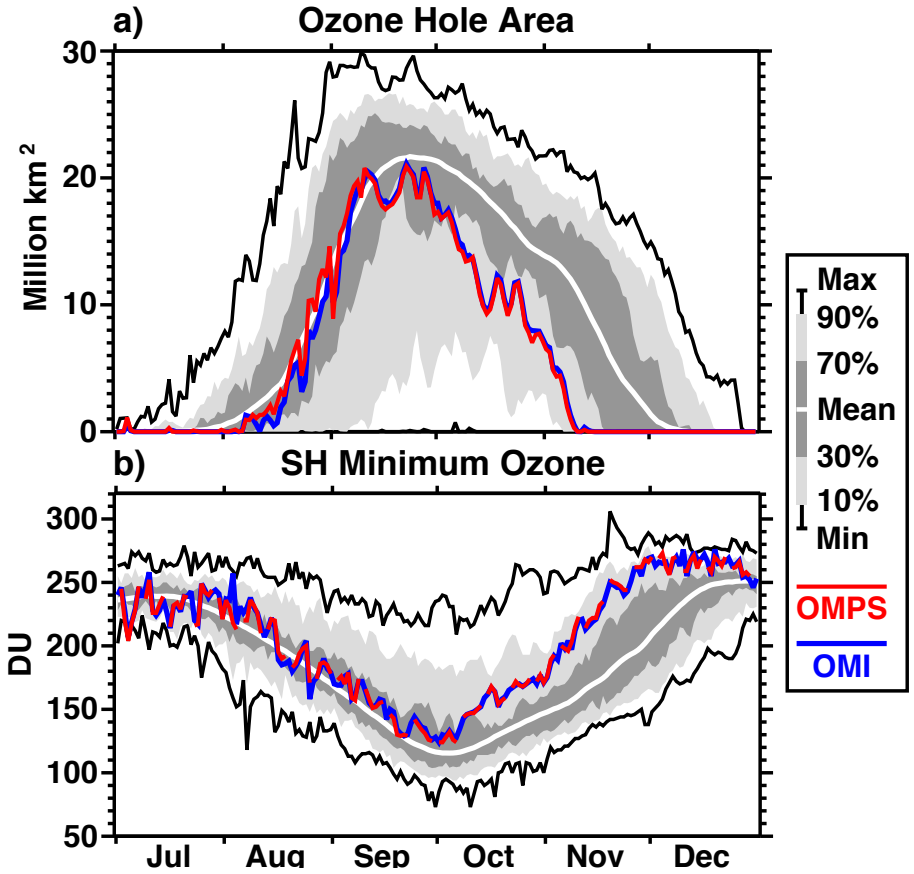

Fig. 5. Ozone hole area **(a)** and minimum ozone **(b)** for OMI (blue) and OMPS TC-NM (red) for 2012. Also shown are the daily climatological distributions for 1979 to 2011: the minimum and maximum (black lines), the 10–90 percentiles (light gray region), the 30–70 percentiles (dark gray region), and the mean (thick white line).

ACPD
13, 26305–26325, 2013

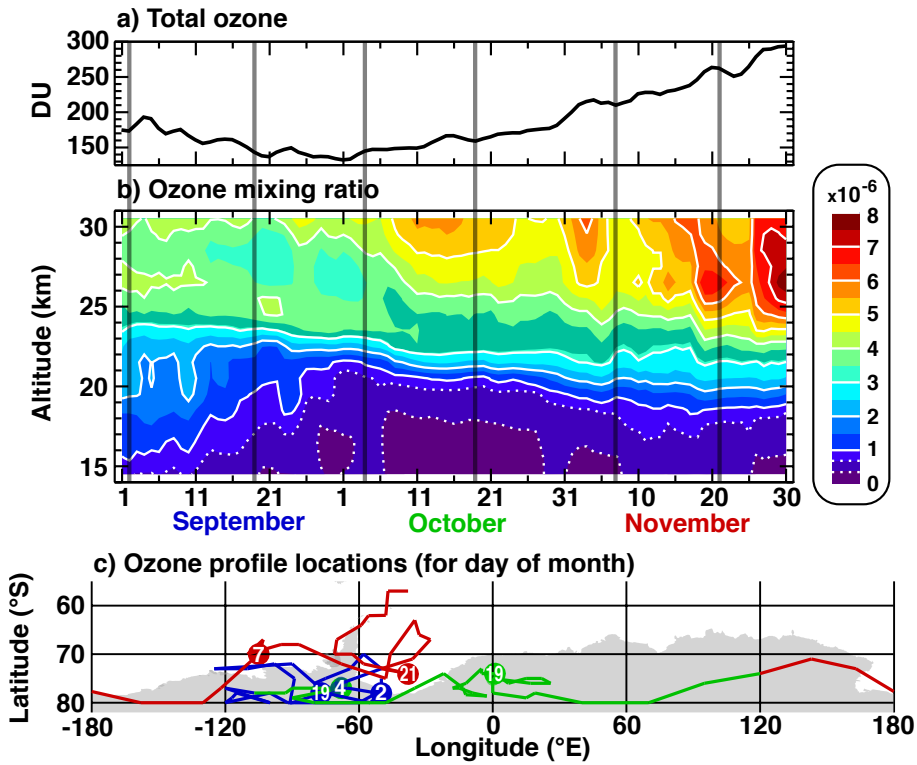

Fig. 6. Total ozone measured from OMPS TC-NM **(a)** and ozone mixing ratios (14.5 km to 30.5 km) from OMPS LP instrument **(b)** for 1 September to 30 November 2012, derived from a location chosen near the center of the polar vortex **(c)**. The chosen locations are connected by colored lines: September, October, and November locations are shown in blue, green, and red, respectively. Vertical gray lines in **(a)** and **(b)** and circles in **(c)** indicate the days 2 September, 19 September, 4 October, 19 October, 7 November, and 21 November. (adapted from Newman et al., 2013, Figure 6.10).

ACPD
13, 26305–26325, 2013

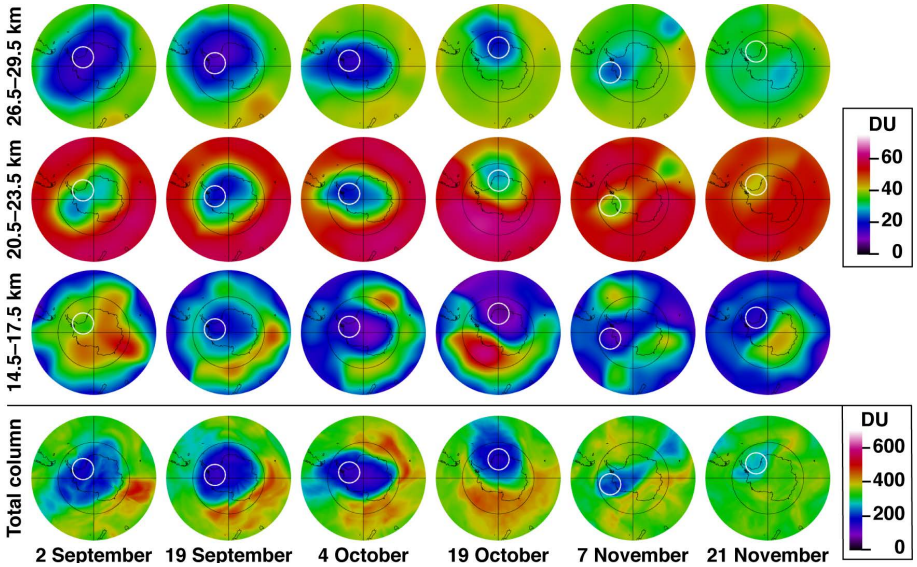

Fig. 7. Column ozone amounts for 3 layers (26.5–29.5 km, 20.5–23.5 km, and 14.5–17.5 km) from OMPS LP and total column ozone amounts from OMPS TC-NM for 2 September, 19 September, 4 October, 19 October, 7 November, and 21 November 2012. The white circles are within a radius of 1000 km of the center of the vortex for that day (see Fig. 6 for how the center of the polar vortex is determined).

ACPD
13, 26305–26325, 2013